E17-2003-53

I. V. Barashenkov, E. V. Zemlyanaya

TRAVELLING SOLITONS IN THE DAMPED DRIVEN NONLINEAR SCHRÖDINGER EQUATION

Submitted to «SIAM Journal of Applied Mathematics»

I. INTRODUCTION

The amplitude of a nearly-harmonic wave propagating in a nonlinear dispersive medium satisfies a nonlinear Schrödinger equation. Confining ourselves to the generic, cubic, nonlinearity of the 'focusing' type, the resulting nonlinear Schrödinger equation is of the form

$$i\Psi_t + \Psi_{xx} + 2|\Psi|^2\Psi = -i\gamma\Psi; \quad \gamma > 0. \tag{1}$$

The $-i\gamma\Psi$ term in the right-hand side accounts for dissipative losses (which were assumed to be small in the derivation of Eq.(1).) In the underlying physical system the dissipation is compensated by pumping the energy into the system, in one way or another. The pumping is modelled by adding a driving term to the right-hand side of Eq.(1).

Like a simple pendulum, the distributed system can be driven externally or parametrically. The typical form of the corresponding amplitude equation is

$$i\Psi_t + \Psi_{xx} + 2|\Psi|^2\Psi = he^{i\Omega t} - i\gamma\Psi, \tag{2}$$

and

$$i\Psi_t + \Psi_{xx} + 2|\Psi|^2\Psi = h\overline{\Psi}e^{2i\Omega t} - i\gamma\Psi, \tag{3}$$

respectively. (The overline in the right-hand side of (3) indicates complex conjugation.) Both the externally and parametrically driven nonlinear Schrödinger equations arise in a great variety of physical contexts. In particular, the parametric equation (3) describes the nonlinear Faraday resonance in a vertically oscillating water tank [1–3] and the effect of phase-sensitive amplifiers on solitons in optical fibers [4]. The same equation controls the magnetisation waves in an easy-plane ferromagnet exposed to a combination of a static and microwave field [5] and the amplitude of synchronised oscillations in vertically vibrated pendula lattices [6].

Both equations (2) and (3) exhibit soliton solutions [7–9], [1, 2, 5], stable and unstable [5, 8], which can also form (stable and unstable) multisoliton complexes [10–12]. All localised solutions that have been found so far, were nonpropagating. In fact, it is widely accepted that the nonlinear Schrödinger solitons simply *cannot* travel in presence of the dissipation. This perception is based on the rate equation

$$\dot{P} = -2\gamma P, \tag{4}$$

which is straightforward from (2) and (3). Here P is the total field momentum,

$$P = \frac{i}{2}\int_{-\infty}^{\infty}(\overline{\Psi}_x\Psi - \Psi_x\overline{\Psi})dx. \tag{5}$$

In the undamped case ($\gamma = 0$) the momentum is conserved; however if $\gamma > 0$, P decays to zero and this seems to suggest that a solitary wave, initially moving with a nonzero velocity, will have to slow down and eventually stop [13].

Another indication that only quiescent solitons are possible in the damped-driven Schrödinger equation, comes ostensibly from the singular [2, 14] and Inverse Scattering-based perturbation theory [7, 15, 16]. Here we should mention however that these techniques are well developed only in the one-soliton sector and in the case of several well separated solitons. They either make use of the smallness of the perturbation in the right-hand side of (2)-(3) [2, 7, 15] or utilise an explicit form of the perturbed soliton (to study its stability and bifurcation) [16]. In any case, the resulting finite-dimensional system of equations for the parameters of the soliton and radiations, leads to the conclusion that the soliton's velocity has to decay to zero as $t \to \infty$.

Meanwhile, the moving solitary waves could play a significant role in a variety of physical situations modelled by the damped-driven nonlinear Schrödinger equations. Stable travelling waves could compete with nonpropagating localised attractors; unstable ones might arise as long-lived transients and intermediate states in spatiotemporal chaotic regimes. Both types of moving solitary waves could mediate energy dissipation in damped-driven systems. One more reason for not rejecting the unstable solutions outright is their possible persistence within the (directly or parametrically driven) Ginzburg-Landau equations of which the damped-driven Schrödinger equations (2)-(3) are special cases [18]. The diffusion and nonlinear damping (the terms $ic_1\Psi_{xx}$ and $-ic_2|\Psi|^{2n}\Psi$, to be added to the right-hand side of (2)-(3)) are known to have a stabilising effect on the Ginzburg-Landau pulses; hence the unstable Schrödinger solitons may gain stability as they are continued to nonzero positive c_1 and c_2.

The purpose of this paper is to show that the damped-driven nonlinear Schrödinger equations do support solitary waves travelling with nonzero velocities. For the demonstration of this fact we confine our study to the *parametrically* driven Schrödinger only. The *externally* driven equation is left as an object of future research.

Two complementary strategies will be pursued to achieve our goal. First, in section III, we consider the *motionless damped* solitons ($V = 0$, $\gamma \neq 0$) and derive the condition under which they can be continued to nonzero velocity. Having identified values of γ for which this condition is satisfied, we perform the numerical continuation obtaining a branch of solitary waves with nonzero V and γ. Our second approach is presented in section IV; the idea is to continue *undamped travelling* waves ($\gamma = 0$, $V \neq 0$) to nonzero dampings. We show that this is only possible if the travelling wave has zero momentum. For complexes with $P = 0$, we then carry out the numerical continuation in γ. In section V we discuss the consistency of results obtained within these two complementary approaches.

We examined, numerically, stability of all solutions obtained within both approaches. The general framework of the stability analysis is outlined in section II. Results of the stability analysis are presented along with results of the numerical continuation. Finally, section VI summarises conclusions of this study.

II. MATHEMATICAL PRELIMINARIES

For purposes of this paper we transform equation (3) to an autonomous form. First, we normalise the driving frequency Ω to unity; after that, the transformation $\Psi(x,t) = e^{it}\psi(x,t)$ takes Eq.(3) to

$$i\psi_t + \psi_{xx} + 2|\psi|^2\psi - \psi = h\overline{\psi} - i\gamma\psi. \tag{6}$$

This is the representation of the parametrically driven damped nonlinear Schrödinger equation that we are going to work with in this paper. We confine ourselves to uniformly travelling solutions of the form

$$\psi(x,t) = \psi(x - Vt) \equiv \psi(\xi), \tag{7}$$

where $\psi(\xi) \to 0$ as $|\xi| \to \infty$. These satisfy an ordinary differential equation

$$-iV\psi_\xi + \psi_{\xi\xi} + 2|\psi|^2\psi - \psi = h\overline{\psi} - i\gamma\psi. \tag{8}$$

The analytical part of this paper deals mainly with identifying those of the previously found solutions of (8) with $V = 0$ or $\gamma = 0$ which can be continued in V and γ, respectively. The actual continuation will be carried out numerically. Our numerical method employs a predictor-corrector continuation algorithm with a fourth-order accurate Newtonian solver. Typically, the infinite line was approximated by an interval $(-100, 100)$. The discretisation stepsize was typically 0.005. The numerical tolerance was set to be 10^{-10}; that is, the grid solution would be deemed accurate if the difference between the left- and right-hand sides in (8) were smaller than 10^{-10}.

Along with the continuation of solutions in V and γ, we will be analysing their stability to small perturbations. To this end, we linearize equation eq.(6) in the co-moving frame of reference. Assuming that the linear perturbation depends on time exponentially,

$$\delta\psi(\xi,t) = e^{\lambda t}\left[\delta u(\xi) + i\delta v(\xi)\right],$$

we arrive at an eigenvalue problem

$$\mathcal{H}_0\,\vec{y} = (\lambda + \gamma)J\,\vec{y}, \tag{9}$$

where the operator $\mathcal{H}_0$ is defined by

$$\mathcal{H}_0 = \begin{pmatrix} -\partial_\xi^2 + 1 + h - 6u^2 - 2v^2 & -V\partial_\xi - 4uv \\ V\partial_\xi - 4uv & -\partial_\xi^2 + 1 - h - 6v^2 - 2u^2 \end{pmatrix}, \tag{10}$$

and the skew-symmetric matrix J is

$$J = \begin{pmatrix} 0 & -1 \\ 1 & 0 \end{pmatrix}.$$

The column vector $\vec{y}(\xi) = (\delta u, \delta v)^T$. The eigenvalue problem (9) was solved by expanding δu and δv over a Fourier basis, typically with 500 modes, on the interval $(-50, 50)$.

The last point that we need to touch upon in this preliminary section, is the integrals of motion of eq.(3), or, more precisely, the quantities which are conserved in the absence of dissipation. When $\gamma = 0$, the equation (3) conserves the momentum (given by eq.(5) where one only needs to replace $\Psi \to \psi$), and energy,

$$E = \int_{-\infty}^{\infty} (|\psi_x|^2 + |\psi|^2 - |\psi|^4 + h\ \mathrm{Re}\,\psi^2)\, dx. \tag{11}$$

In the damped case, the momentum decays according to the rate equation (4) while the energy satisfies

$$\dot{E} = 2\gamma \left(\int_{-\infty}^{\infty} |\psi|^4 dx - E \right). \tag{12}$$

III. CONTINUATION OF DAMPED SOLITONS TO NONZERO VELOCITIES

A. Continuability criterion

Our first strategy is to attempt to continue stationary solutions with nonzero γ to nonzero V. Two basic soliton solutions, denoted ψ_+ and ψ_-, are available explicitly:

$$\psi_\pm(x) = e^{-i\theta_\pm} A_\pm \,\mathrm{sech}\,(A_\pm x); \tag{13}$$
$$A_\pm = \sqrt{1 \pm \sqrt{h^2 - \gamma^2}},$$
$$\theta_+ = \frac{1}{2} \arcsin \frac{\gamma}{h}, \quad \theta_- = \frac{\pi}{2} - \theta_+.$$

The two solitons can form a variety of stationary complexes. These are denoted, symbolically, $\psi_{(++)}$, $\psi_{(--)}$, $\psi_{(+-+)}$, $\psi_{(-+-)}$, and so on [12]. Let $\psi_0(x)$ be a particular complex; we want to find out whether it can be continued in V. Assuming there is a solution $\psi(\xi; V)$ such that $\psi(\xi; 0) \equiv \psi_0(\xi)$ $(= \psi_0(x))$, we expand $\psi(\xi; V)$ in powers of V as

$$\psi(\xi; V) = e^{-i\theta} \{\, u_0(\xi) + iv_0(\xi) + V[u_1(\xi) + iv_1(\xi)] + V^2[u_2(\xi) + iv_2(\xi)] + \ldots \}, \tag{14}$$

where the constant phase θ will be chosen at a later stage. We also expand h and γ: $h = h_0 + h_1 V + \ldots$, $\gamma = \gamma_0 + \gamma_1 V + \ldots$. Substituting into (8), the order V^1 gives

$$\mathcal{L} \begin{pmatrix} u_1 \\ v_1 \end{pmatrix} = \begin{pmatrix} v_0' \\ -u_0' \end{pmatrix} + \mathcal{B} \begin{pmatrix} u_0 \\ v_0 \end{pmatrix}, \tag{15}$$

where the operator $\mathcal{L}$ has the form

$$\mathcal{L} = \begin{pmatrix} -\partial_x^2 + 1 + h_0 \cos 2\theta - 6u_0^2 - 2v_0^2 & \gamma_0 + h_0 \sin 2\theta - 4u_0 v_0 \\ -\gamma_0 + h_0 \sin 2\theta - 4u_0 v_0 & -\partial_x^2 + 1 - h_0 \cos 2\theta - 2u_0^2 - 6v_0^2 \end{pmatrix}; \tag{16}$$

the constant matrix $\mathcal{B}$ is given by

$$\mathcal{B} = \begin{pmatrix} -h_1 \cos 2\theta & -\gamma_1 - h_1 \sin 2\theta \\ \gamma_1 - h_1 \sin 2\theta & h_1 \cos 2\theta \end{pmatrix},$$

and the primes over u_0 and v_0 indicate derivatives with respect to x. (In (15) and (16) we have replaced ξ with x as ξ coincides with x for $V = 0$.) According to Fredholm's alternative, eq.(15) has a bounded solution $u_1(x), v_1(x)$ iff the vector in the right-hand side is orthogonal to the kernel of the Hermitean-conjugate operator $\mathcal{L}^\dagger$:

$$\int (y, w) \begin{pmatrix} v_0' \\ -u_0' \end{pmatrix} dx + \int (y, w)\, \mathcal{B} \begin{pmatrix} u_0 \\ v_0 \end{pmatrix} dx = 0. \tag{17}$$

Here $\vec{y}(x) = (y, w)^T$ is the eigenvector of $\mathcal{L}^\dagger$ associated with the zero eigenvalue: $\mathcal{L}^\dagger \vec{y} = 0$. That the operator $\mathcal{L}^\dagger$ has a zero eigenvalue follows from the fact that the operator $\mathcal{L}$ has one, namely, the translation eigenvalue corresponding to the eigenvector $(u_0', v_0')^T$. Eq.(17) gives a necessary continuability condition of damped queiscent solitons to nonzero velocities.

B. Noncontinuability of the 'building blocks'

It is quite easy to check that when $\gamma_0 \neq 0$, the individual ψ_+ and ψ_- solitons (the basic 'building blocks' of which all complexes are constructed) are *not* continuable to nonzero V. Choosing $\theta = \theta_+$ for the ψ_+ soliton and $\theta = \theta_-$ for the ψ_- (where $\theta_\pm$ are to be computed from the bottom formula in (13) with $\gamma = \gamma_0$ and $h = h_0$), we get $v_0(x) = 0$, $\gamma_0 - h_0 \sin 2\theta = 0$ and so the 2×2 matrix $\mathcal{L}$, eq.(16), becomes upper triangular. The zero mode of $\mathcal{L}^\dagger$ can now be readily found.

Consider, for instance, the ψ^+ case. The zero mode satisfies

$$\begin{pmatrix} -\partial_x^2 + A_+^2 - 6u_0^2 & 0 \\ 2\gamma_0 & -\partial_x^2 + A_-^2 - 2u_0^2 \end{pmatrix} \begin{pmatrix} y \\ w \end{pmatrix} = 0,$$

hence $y(x) = u_0'(x)$ and $w(x)$ is found from

$$(-\partial_x^2 + A_-^2 - 2u_0^2) w = -2\gamma u_0'(x). \tag{18}$$

Using the explicit expression for $u_0(x)$, $u_0(x) = A_+ \mathrm{sech}(A_+ x)$, the operator in the left-hand side of (18) can be written as $A_+^2(L_0 - \epsilon)$, where $\epsilon = 2h_0 \cos(2\theta_+)/A_+^2$; L_0 is given by

$$L_0 = -\partial_X^2 + 1 - 2\mathrm{sech}^2 X,$$

and $X = A_+ x$. The operator L_0 has familiar spectral properties; in particular it has a single discrete eigenvalue $E_0 = 0$ associated with an even eigenfunction $z_0 = \mathrm{sech} X$, while its continuous spectrum occupies the semiaxis $E_k \geq 1$. Consequently, for $0 < \epsilon < 1$ (that is, for $h_0 < \sqrt{1 + \gamma_0^2}$), the operator $L_0 - \epsilon$ is invertible and a bounded solution $w(x)$ of (18) exists and is unique. It can be found explicitly, but

this is not really necessary for our purposes. All we need to know is that, since L_0 is a parity-preserving operator, $w(x)$ has the same parity as the right-hand side in (18), i.e. it is an odd function. For that reason the second integral in equation (17) vanishes and the necessary continuability condition reduces to

$$\gamma \int u_0'(x)(L_0 - \epsilon)^{-1} u_0'(x) dx = 0. \tag{19}$$

This quadratic form can be easily evaluated by expanding $u_0'(x)$ over eigenfuctions of the operator L_0:

$$u_0'(x) = \int_{-\infty}^{\infty} U(k) z_k(X) dk,$$

where $L_0 z_k(X) = (1+k^2) z_k(X)$. (The 'discrete' eigenfunction $z_0(X)$ does not appear in the expansion as it has the opposite parity to $u_0'(x)$.) Utilising the orthonormality of the eigenfunctions, the continuability condition (19) is transformed into

$$\gamma \int \frac{|U(k)|^2}{k^2 + 1 - \epsilon} dk = 0. \tag{20}$$

As $\epsilon < 1$, this condition can obviously not be satisfied (unless $\gamma = 0$).

In the case of the ψ_- soliton the analysis is similar. In this case the continuability condition (20) is replaced by

$$\gamma \int \frac{|U(k)|^2}{k^2 + (1 - \epsilon)^{-1}} dk = 0,$$

and this cannot be met for the same reason as eq.(20).

C. Continuation of the complexes

Turning to the *complexes* of the solitons ψ_+ and ψ_-, the phase of the complex varies with x and therefore the matrix $\mathcal{L}$ cannot be made triangular no matter how we choose the constant θ in (14). For this reason, aggravated by the fact that the multisoliton solutions are not available explicitly, the continuability condition (17) cannot be verified analytically. Resorting to the help of computer, we evaluated the eigenfuction $\vec{y}(x)$ associated with the zero eigenvalue of the operator $\mathcal{L}^\dagger$ numerically.

All damped soliton complexes found in [12], were symmetric; that is, the corresponding u and v are *even* functions of x. Therefore, the operator $\mathcal{L}^\dagger$ whose potential part is made up of $u(x)$ and $v(x)$, is parity preserving and all its eigenfunctions pertaining to nonrepeated eigenvalues are either even or odd. As we move along a continuous branch of solutions, the parity of the eigenfunction has to change continuously. Since the parity equals either $+1$ (for even functions) or -1 (for odd functions), the only option left to it by the continuity argument, is to remain constant on the entire branch. For that reason it is sufficient to determine the parity of the eigenfunction for one specific value of h — and we will know it at all other

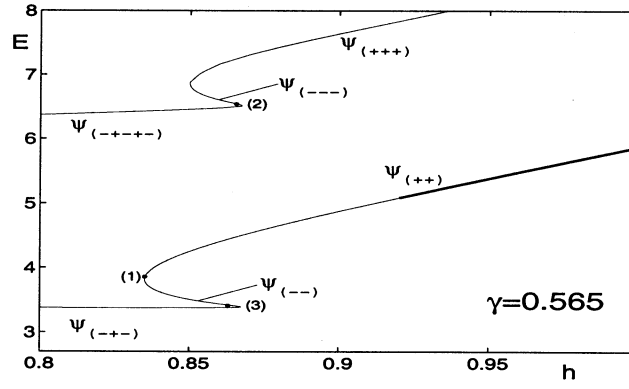

Fig. 1. A fragment of the bifurcation diagram for stationary multisoliton complexes (adapted from [12].) Shown is the energy (11) of the complex as a function of h. The bottom branch pertains to symmetric two-soliton complexes $\psi_{(++)}$ and $\psi_{(--)}$ and a three-soliton solution $\psi_{(-+-)}$; the top branch includes the three-soliton states $\psi_{(+++)}$ and $\psi_{(---)}$, as well as a five-soliton solution $\psi_{(-+-+-)}$. The thick curve corresponds to stable and thin curves to unstable solutions. The black dots indicate points where the integral (21) equals zero and therefore moving solitons are allowed to bifurcate off.

points. Our numerical calculation shows that the eigenfunction $\vec{y}(x)$ is *odd* on all branches reported in [12]. Consequently, the second term in (17) is always zero and we only need to evaluate the first term.

Having found the solution $\psi(x) = u(x) + iv(x)$ at representative points along each branch, we obtained the eigenfunction $\vec{y}(x)$ at these points and evaluated what remains of the integral (17):

$$\int (yv_0' - wu_0')\, dx \equiv I(h). \tag{21}$$

The integral I is a continuous function of h, and it was not difficult to find points on the curve at which it changes from positive to negative values, or vice versa.

We examined two branches of multisoliton solutions obtained previously [12] (Fig.1). The integral $I(h)$ was found to change its sign at three points, marked by black dots in Fig.1. (Although it may seem from the figure that I equals zero right at the turning points, in the actual fact zeros of I do not *exactly* coincide with the turning points.) We were indeed able to numerically continue our solutions in V from each of these three points. Results are presented in Fig.2, (a)-(c).

The point '1' in Fig.1 corresponds to the stationary complex $\psi_{(++)}$ and lies just above the turning point where the $\psi_{(++)}$ turns into $\psi_{(--)}$. (The turning point has $h = 0.83504217$ while $I(h) = 0$ for $h = 0.8353$.) This solution has four positive real eigenvalues in the spectrum of the associated linearised operator and hence is unstable. The $\gamma(V)$ curve which results from the continuation of this solution in

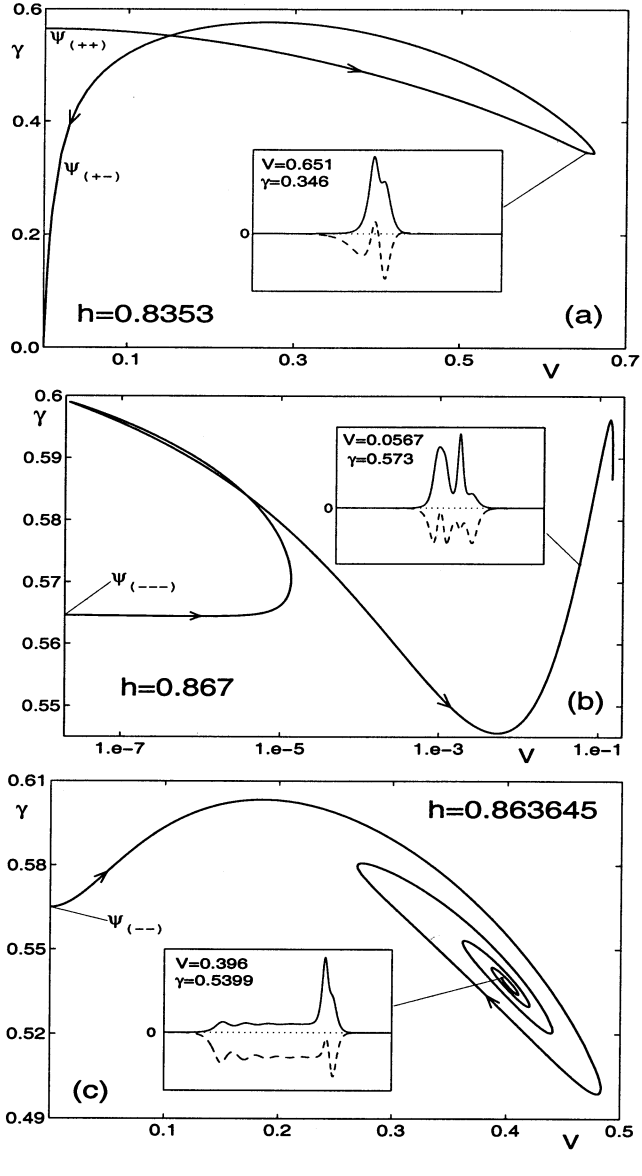

Fig. 2. Bifurcation curves branching off the points marked by black dots in Fig.1. The curves illustrate the relation between the value of the damping γ and velocity V at which the wave may travel for that γ. Each curve begins at the point $\gamma = 0.565$ on the vertical axis. The insets show representative solutions at internal points of each branch. (Solid line: real part; dashed line: imaginary part.) Note the logarithmic scale of V in (b). Here, and in all other diagrams, arrows indicate our direction of continuation.

V, is shown in Fig.2(a). As V grows from zero, the solution looses its even symmetry (see the inset to Fig.2(a)) while the four positive eigenvalues collide, pairwise, and become two complex conjugate pairs with positive real parts. After reaching a maximum velocity of approximately 0.65, the curve turns back towards $V = 0$, with γ first growing but then also turning towards $\gamma = 0$. The solution transforms into a (strongly overlapped) $\psi_{(+-)}$ complex. As V and γ tend to their zero values, the separation between the ψ_+ and ψ_- constituent solitons in the complex grows to infinity. The spectrum becomes the union of the eigenvalues of the individual ψ_+ and ψ_- solitons; in particular, it includes a complex-conjugate pair with positive real part, and a positive real eigenvalue. Thus the entire branch shown in Fig.2(a) is unstable.

One more comment that we need to make here, concerns the validity of the continuation scenario presented in Fig.2(a) for other values of h. Note that if we chose a smaller value of γ in Fig.1, the value of h corresponding to the point '1' would also be smaller. (For example, taking $\gamma = 0.548$ gives $h = 0.82$.) For this smaller h the final product of the continuation turns out to be not a pair of infinitely separated stationary ψ_+ and ψ_- but a totally different complex. This is discussed below in section V; see also Figs.4(c) and 5.

Another branch bifurcates off at the point marked '2' in Fig.1. Here $h = 0.867$. The corresponding $\gamma(V)$ diagram is displayed in Fig.2(b). As we move along the branch departing from $V = 0$, the original stationary complex $\psi_{(---)}$ transforms into a solution displaying three widely separated peaks in its real part: one corresponding to a strongly overlapping complex $\psi_{(-+-)}$; the next one to the ψ_+ and the last one to the ψ_- soliton. After passing a turning point, the curve is reapproaching, tangentially, the $V = 0$-axis. However, having reached $V = 2.2 \times 10^{-8}$, it suddenly turns back and the velocity starts to grow again. The separation between the solitons decreases and the solution can now be interpreted as a strongly overlapping four-soliton complex $\psi_{(+++-)}$ (shown in the inset to Fig.2(b)). As we continue further, the four constituent solitons regroup into two complexes, $\psi_{(++)}$ and $\psi_{(+-)}$. The distance between the two complexes grows rapidly and, for certain finite V and γ (at the endpoint of the curve in Fig.2(b)) becomes infinite. At this point we have two coexisting solutions, $\psi_{(++)}$ and $\psi_{(+-)}$, and so this point corresponds to the point of self-intersection of the curve shown in Fig.2(a). Continuing the two solutions, separately, from the endpoint of the curve in Fig.2(b), we reproduce the diagram of Fig.2(a) for a slightly different value of h (i.e. for $h = 0.867$.)

The entire branch shown in Fig.2 (b) is unstable. The start-off stationary solution $\psi_{(---)}$ has three positive real eigenvalues in its spectrum; one of these persists for all V and γ while the other two collide and form a complex-conjugate pair with positive real part.

The branch continuing from the point '3' in Fig.1, for which $h = 0.863645$, leads to the least expected solutions. The resulting $\gamma(V)$ curve is shown in Fig.2(c). For points lying on the 'spiral' part of the curve, the function $\psi(x)$ is equal to a constant in a relatively large but finite region, and zero outside that region. (See the inset to Fig.2(c).) The constant is $\psi^{(0)} = (A_-/\sqrt{2})e^{-i\theta_-}$; it defines a stationary spatially

uniform solution to eq.(6). (This flat background is unstable with respect to the continuous spectrum perturbations. Figuratively speaking, our pulse solution $\psi(x)$ represents a 'droplet' of the unstable phase in the stable one.) On one side (at the rear of the pulse) the zero background is connected to the background $\psi^{(0)}$ by a kink-like interface. In the front of the pulse, the interface has the character of a large-amplitude excitation, with the shape reminding the $\psi_{(+-)}$ complex. As the curve $\gamma(V)$ spirals towards its 'focus' in Fig.2(c), the length of the region where $\psi(x) = \psi^{(0)}$ is growing. The entire branch is unstable; the start-off $\psi_{(--)}$ solution already has two real positive eigenvalues in its spectrum and more appear as we move along the branch. Those additional positive eigenvalues are remnants of the unstable interval of the continuous spectrum of the flat nonzero solution $\psi^{(0)}$.

IV. CONTINUATION OF TRAVELLING WAVES TO NONZERO DAMPINGS

A. Continuability conditions

When $\gamma = 0$, the equation (8) has a plethora of localised solutions with nonzero V [17], and our second strategy will be to attempt to continue these undamped travelling waves to nonzero γ. We start with establishing the necessary and sufficient conditions for such a continuation.

A set of the *necessary* conditions can be easily derived using two integral characteristics of equation (6), the momentum $P = (i/2)\int(\overline{\psi}_x\psi - \psi_x\overline{\psi})dx$, and energy (11). No matter whether γ equals zero or not, the uniformly travelling solitary waves (i.e. solutions of the form (7)) satisfy $\dot{P} = \dot{E} = 0$. Using these relations in eqs.(4) and (12) with $\gamma \neq 0$, we get

$$P = 0, \tag{22}$$

and

$$E = \int |\psi|^4 dx. \tag{23}$$

Equations (22)-(23) have to be satisfied by the undamped solutions continuable to nonzero γ.

In fact, eqs.(22) and (23) are not independent. Indeed, multiplying Eq.(8) by $\overline{\psi}$, adding its complex conjugate and integrating, gives an identity

$$E - \int |\psi|^4 dx = VP. \tag{24}$$

Letting $P = 0$ in (24), eq.(23) immediately follows. Thus we can keep equation $P = 0$ as the *only* necessary condition for the continuability to nonzero γ; eq.(23) is satisfied as soon as eq.(22) is in place.

It turns out that $P = 0$ is also a *sufficient* condition. To show this, we expand the field $\psi = u + iv$ in powers of γ:

$$u = u_0 + \gamma u_1 + \gamma^2 u_2 + ..., \quad v = v_0 + \gamma v_1 + \gamma^2 v_2 + ...,$$

substitute into (8) and equate coefficients of like powers. At the order $\mathcal{O}(\gamma^1)$, we obtain:

$$\mathcal{H}_0 \begin{pmatrix} u_1 \\ v_1 \end{pmatrix} = \begin{pmatrix} -v_0 \\ u_0 \end{pmatrix}. \tag{25}$$

Here the hermitean operator $\mathcal{H}_0$ is as in (10) where we only need to attach zero subscripts to u and v:

$$\mathcal{H}_0 = \begin{pmatrix} -\partial_\xi^2 + 1 + h_0 - 6u_0^2 - 2v_0^2 & -V_0\partial_\xi - 4u_0v_0 \\ V_0\partial_\xi - 4u_0v_0 & -\partial_\xi^2 + 1 - h_0 - 2u_0^2 - 6v_0^2 \end{pmatrix}. \tag{26}$$

Since the operator $\mathcal{H}_0$ has a zero eigenvalue, with the translation mode as an associated eigenvector, equation (25) is only solvable if its right-hand side is orthogonal to (u_0', v_0'):

$$\int (u_0', v_0') \begin{pmatrix} -v_0 \\ u_0 \end{pmatrix} d\xi = P = 0.$$

(Here the prime indicates the derivative with respect to ξ.)

Assume $P = 0$ so that a bounded solution to (25) exists. All travelling waves found in [17] have even real and odd imaginary parts: $u_0(-x) = u_0(x)$, $v_0(-x) = -v_0(x)$. Noticing that the diagonal elements of the operator $\mathcal{H}_0$ are parity-preserving while the off-diagonal elements change their sign under the $\xi \to -\xi$, we conclude that $u_1(x)$ is odd and $v_1(x)$ is even.

Proceeding to the order $\mathcal{O}(\gamma^2)$, we have

$$\mathcal{H}_0 \begin{pmatrix} u_2 \\ v_2 \end{pmatrix} = \begin{pmatrix} -v_1 + u_0[6u_1^2 + 2v_1^2] + 4v_0u_1v_1 \\ u_1 + v_0[2u_1^2 + 6v_1^2] + 4u_0u_1v_1 \end{pmatrix}. \tag{27}$$

The top entry in the right-hand side of (27) is even and the bottom one odd; hence the right-hand side is orthogonal to the null vector (u_0', v_0') and a bounded solution $u_2(\xi), v_2(\xi)$ exists. This time the u-component is even and the v-component odd: $u_2(-\xi) = u_2(\xi)$, $v_2(-\xi) = -v_2(\xi)$.

It is not difficult to verify that this parity alternation property guarantees the boundedness of $u_n(\xi)$ and $v_n(\xi)$ for all n. Therefore, equation (8) has a localised solution ($\psi(\xi) \to 0$ as $|\xi| \to \infty$) for sufficiently small γ. Thus if we have an undamped soliton travelling with zero momentum, it can be continued to nonzero values of γ.

B. Continuable solutions: the bifurcation diagram of the undamped nonlinear Schrödinger

In this subsection we review the $P(V)$ dependence for the undamped solitons and solitonic complexes [17]. Of interest, of course, are points where the graph crosses the V-axis, i.e. where $P(V) = 0$.

The simplest solutions arising for $V = 0$ are, obviously, our stationary fundamental solitons ψ_+ and ψ_-. These are given by eqs.(13) where one only needs to set $\gamma = 0$:

$$\psi_+(x) = A_+ \mathrm{sech}\,(A_+x), \quad \psi_-(x) = iA_- \mathrm{sech}\,(A_-x),$$

with $A_\pm^2 = 1 \pm h$. Both ψ_+ and ψ_- have zero momenta and therefore, are continuable to nonzero γ. However, the continuation does not produce any travelling waves in this case; all we get is our static damped solitons $\psi_\pm$, Eq.(13).

Next, both ψ_+ and ψ_- admit continuation to nonzero V (for the fixed $\gamma = 0$) [17]. As V is increased to

$$c = \sqrt{2 + 2\sqrt{1 - h^2}},$$

the width of the soliton ψ_- increases, its amplitude decreases and the soliton gradually transforms into the trivial solution, $\psi \equiv 0$. On the resulting branch, the momentum vanishes only for $V = 0$ and $V = c$ and therefore, no damped branches can bifurcate off the travelling ψ_- soliton.

We now turn to the soliton ψ_+. When $h < 0.28$, its fate is similar to that of the ψ_-: as $V \to c$, the soliton spreads out and merges with the zero solution. The momentum equals zero only at two points, $V = 0$ and $V = c$; for $0 < V < c$, the momentum is positive.

For $h > 0.28$, the transformation of the ψ_+ is more promising from the present viewpoint (see the dashed curve in Fig.3). As V is increased from zero, the momentum grows, then the branch turns back towards the $V = 0$ axis. For some $V < 0$ the momentum reaches its maximum and then decreases to zero. The point $V = V_1$ where $P(V_1) = 0$ is of interest to us as a branch of damped solitons can bifurcate off at this point (and it really does, see subsection IV D.) Continuing beyond V_1, the curve $P(V)$ turns towards $V = 0$ and then, after one more turning point, we have another zero crossing: $P(V_2) = 0$. This is how far we have managed to advance in our previous work [17].

At this point we need to mention that the ψ_+ and ψ_- are not the only quiescent solitons for $\gamma = 0$. The dashed $P(V)$ curve in Fig.3 is seen to have one more intersection with the P axis, apart from the one at the origin. The corresponding solution represents a symmetric strongly overlapping complex of the ψ_+ and ψ_- solitons and was coined "twist"(symbolically ψ_T) in [17]. The twist soliton arises both for h greater and smaller than 0.28. In the former region the twist obtains from the V-continuation of the ψ_+ soliton while for $h < 0.28$, it is not connected to the ψ_+. (See the solid curve in Fig.3.) The continuation of the twist in V in the case $h < 0.28$ gives rise to a new branch of the undamped solutions which has a point of intersection with the $P = 0$ axis, at some $V = V_1$. A damped travelling wave is bifurcating off at this value of velocity; see the next subsection. We are using the same notation V_1 in the small- and large-h case in Fig.3 to emphasise the similarity of the resulting $\gamma(V)$ curves in the two cases (forthcoming).

Returning to the case of large h, the entire dashed curve in Fig.3 corresponds to symmetric solutions: $\psi(-\xi) = \overline{\psi}(\xi)$. It turns out that there are also nonsymmetric solutions; these were missed in [17]. The real part of a nonsymmetric solution is not even and imaginary part not odd. In particular, a pair of asymmetric solutions arise in a pitchfork bifurcation of the complex $\psi_{(TT)}$; see the dash-dotted offshoot from the dashed curve in Fig.3. (The two asymmetric solutions are related by the transformation $\psi(\xi) \to \overline{\psi}(-\xi)$; they obviously have equal momenta and hence are represented by the same curve.) Continuing the asymmetric branch we have the

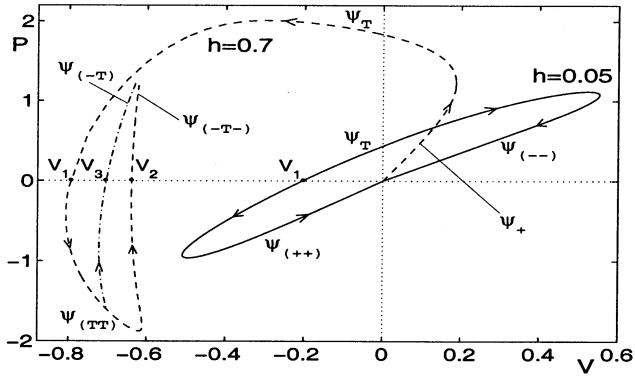

Fig. 3. The momentum of the undamped travelling wave as a function of its velocity (a combined and advanced version of two diagrams from [17]). The dashed and dash-dotted curves pertain to the case of large driving strengths (here exemplified by $h = 0.7$). The starting point $P = V = 0$ of the dashed curve corresponds to the stationary undamped ψ_+ soliton, which then transforms to the twist, then to a bound state of two twists and then to a complex of a twist and two ψ_- solitons. (This curve appeared in [17].) The dash-dotted offshoot is our new contribution to the diagram; it corresponds to an asymmetric solution, $\psi_{(-T)}$, detaching from the $\psi_{(TT)}$ curve. The solid curve pertains to the case of small driving amplitudes (here $h = 0.05$). (This curve also appeared in [17].) The points of its intersection with the P-axis correspond to stationary twist solitons; continuing each of these counterclockwise gives rise to a bound state of two ψ_+'s, while when continued clockwise each twist transforms into a complex of two ψ_-'s. More solution curves can be generated by the mapping $V \to -V$, $P \to -P$.

third zero crossing, at $V = V_3$. When continued to positive P, the asymmetric solution acquires the form of a complex of ψ_- and ψ_T solitons, with the intersoliton separation growing as P is increased. (Note that although the dashed and dash-dotted curve end at nearby points, they are *not* connected.) Our numerical analysis shows that branches of damped solitons do indeed detach at V_1, V_2 and V_3; these will be described in the next two subsections.

C. Numerical continuation: Small driving amplitudes

For small h, $h < 0.28$, our continuation departs from the twist soliton moving with the velocity V_1 (the point of intersection of the solid curve with the horisontal axis in Fig.3.) The real part of this solution is even and imaginary part odd: $\psi(-x) = \overline{\psi}(x)$. As we continue to nonzero γ, this symmetry is lost; a typical profile at the internal points looks like a nonsymmetric complex of the ψ_- and ψ_+ and is displayed in the inset to Fig.4(a). The rest of Fig.4(a) shows the resulting $\gamma(V)$ dependence. As γ grows, the negative velocity of the travelling wave decreases in modulus. However

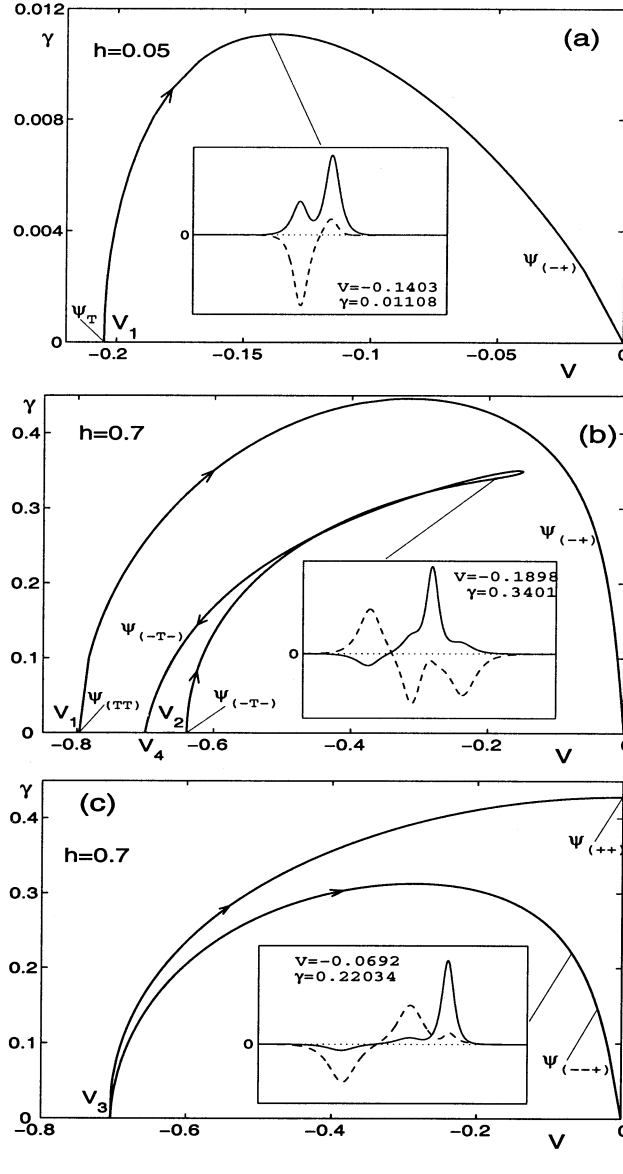

Fig. 4. Results of the numerical continuation of the undamped travelling solitons to nonzero γ. (a): small h; (b),(c): large h. The inset displays a representative solution at one of the internal points of the curve. (Solid line: real part; dashed line: imaginary part.) Each curve shown has a positive-velocity counterpart which arises by the mirror reflection $V \to -V$ of the figure.

the damping cannot be increased beyond a certain limit value; as we reach it, the $\gamma(V)$-curve turns down (Fig.4(a)). As V and γ tend to zero, the separation between the ψ_- and ψ_+ solitons in the complex grows without bounds.

These transformations of the solution are reflected by the behaviour of the linearised eigenvalues in the eigenvalue problem (9). At the point $V = V_1$, $\gamma = 0$ of the $\gamma(V)$ curve, the twist solution has a quadruplet of complex eigenvalues $\pm\lambda, \pm\overline{\lambda}$ which dissociates into two pairs of complex-conjugate eigenvalues $\lambda_1, \overline{\lambda}_1$ and $\lambda_2, \overline{\lambda}_2$ (with $\mathrm{Re}\,\lambda_1 < 0$ and $\mathrm{Re}\,\lambda_2 > 0$) as γ deviates from zero. As we move towards the maximum of the curve, the imaginary parts of λ_1 and λ_2 decrease and the four complex eigenvalues move onto the real axis. At the point of maximum one of the resulting two positive eigenvalues crosses to the negative real axis, but the other one persists all the way to $V = 0-$ and $\gamma = 0+$. Therefore the spectrum of eigenvalues on the 'downhill' portion of the curve is a union of eigenvalues of the ψ_- and ψ_+ solitons. The conclusion of the eigenvalue analysis is that the travelling complex whose bifurcation diagram is exhibited in Fig.4(a), is unstable for all V and γ.

D. Numerical continuation: Large driving amplitudes

For $h > 0.28$ we have three starting points with $P = 0$ corresponding to two intersections of the dashed curve and one of the dash-dotted curve with the horisontal axis in Fig.3.

The $\gamma(V)$ curve emanating out of the point V_1 is the top, arc-shaped, curve in Fig.4(b). For $V = V_1$ and $\gamma = 0$ the solution is symmetric and its shape reminds two strongly overlapping twists. The linearised spectrum includes two complex quadruplets. As γ deviates from zero, the symmetry is lost and the solution starts looking like an asymmetric complex of two pulses. The two quadruplets of eigenvalues become four complex-conjugate pairs, two with positive and two with negative real parts. Two of these pairs (one with $\mathrm{Re}\,\lambda > 0$ and one with $\mathrm{Re}\,\lambda < 0$) move on to the real axis. After that one positive real eigenvalue crosses to the negative semiaxis, while the complex pair with $\mathrm{Re}\,\lambda > 0$ crosses into the $\mathrm{Re}\,\lambda < 0$ half-plane but then returns to $\mathrm{Re}\,\lambda > 0$. As $V, \gamma \to 0$, the separation between the ψ_- and ψ_+ solitons comprising this complex increases, and eventually the two constituents diverge to infinities. On the 'downhill' portion of the curve, the spectrum is a union of the spectra of the individual ψ_- and ψ_+ solitons; in particular, it includes a positive real eigenvalue and a complex quadruplet. Since there are eigenvalues with $\mathrm{Re}\,\lambda > 0$ for all V, the entire branch is unstable.

The second undamped travelling wave with zero momentum (point V_2 on the bifurcation diagram Fig.3) corresponds to a symmetric $[\psi(-x) = \overline{\psi}(x)]$ complex of two ψ_- and one twist soliton, symbolically $\psi_{(-T-)}$. The spectrum includes three complex quadruplets. As we continue in γ and V, the symmetry is lost but the solution still looks like a complex of three solitons, see the inset to Fig.4(b). The bottom, spike-shaped, curve in Fig.4(b) depicts the corresponding $\gamma(V)$ dependence. Unlike the branch starting at the value $V = V_1$, this solution cannot be continued to zero velocities. Instead, the $\gamma(V)$ curve turns back and, as γ approaches zero

from above, V tends to a negative value V_4, with $|V_4| > |V_2|$. For sufficiently small γ the corresponding solution consists of two ψ_- solitons and a twist in between, with the intersoliton separations growing to infinity as $\gamma \to 0$, $V \to V_4$. The associated eigenvalues perform rather complicated movements on the complex plane; skipping the details it suffices to mention that 'unstable' eigenvalues (real positive or complex with positive real parts) are present for all V. Hence the entire branch is unstable.

Finally, the point V_3 on the diagram Fig.3 represents *two* nonequivalent asymmetric solutions with zero momentum, $\psi_1(\xi)$ and $\psi_2(\xi)$, with $\psi_2(\xi) \equiv \overline{\psi}_1(-\xi)$. Consequently, there are *two* distinct $\gamma(V)$-branches coming out of this point (Fig.4(c)). One of these corresponds to a complex of two solitons; when continued to $V = 0$, it gives rise to the symmetric complex $\psi_{(++)}$ with nonzero γ. (See the top curve in Fig.4(c)). Continuing the other asymmetric solution to $V = 0$, the corresponding value of γ reaches a maximum at $V \sim 0.3$ and then tends to zero. (The bottom curve in Fig.4(c)). For sufficiently small V and γ this solution represents a complex $\psi_{(--+)}$ (shown in the inset to Fig.4(c)). As $V, \gamma \to 0$, the intersoliton separation tends to infinity. Turning to the eigenvalues, the start-off solution at the point V_3 has two complex quadruplets and a real positive eigenvalue in its spectrum. When we continue along the top curve in Fig.4(c), two complex eigenvalues move on to the positive real axis, so we end up with three positive eigenvalues. When we continue along the bottom curve, the movements of the eigenvalues are more involved but some of them always remain in the unstable half-plane $\mathrm{Re}\,\lambda > 0$. The upshot of the eigenvalue analysis is that both curves represent only unstable solutions.

V. CONSISTENCY OF THE TWO APPROACHES

To complete our classification of damped travelling solitons, we need to comment on what may seem to be an inconsistency between results obtained within the above two complementary approaches. The solution representing the well-separated ψ_+ and ψ_- solitons reported in sections III and IV, can be reached by continuing both off the ($\gamma = 0$)- and ($V = 0$)-axes. (This branch connecting to the origin on the (V, γ)-plane appears both in Figs. 2(a) and 4(b).) Although such a curve should obviously not depend on the starting point of the continuation, one notices that the $\psi_{(+-)}$ branches 'flowing into the origin' in Figs. 2(a) and 4(b) behave differently when traced backwards (i.e. away from $V = \gamma = 0$). While the curve in Fig.2(a) intersects the γ-axis, its counterpart in Fig.4(b) crosses the other, V-, axis. (Here the reader should not be confused by the fact that the $\psi_{(+-)}$ branch in Fig.2(a) is shown for positive and its counterpart in Fig.4(b) for negative values of V. In view of the $\xi \to -\xi$, $V \to -V$ invariance of equation (8), to each γ there correspond *two* travelling waves, one with positive and the other one with negative value of V. Therefore, one should mirror-reflect Fig.4(b) prior to comparing it to Fig.2(a). This reflection maps the solution $\psi_{(-+)}$ of Fig.4(b) to the $\psi_{(+-)}$ of Fig.2(a).)

To resolve the paradox, one needs to note that the two figures correspond to different values of h, Fig.2(a) to $h = 0.8353$ and Fig.4(b) to $h = 0.7$. It turns out that a qualitative change of behaviour occurs for h somewhere between these values,

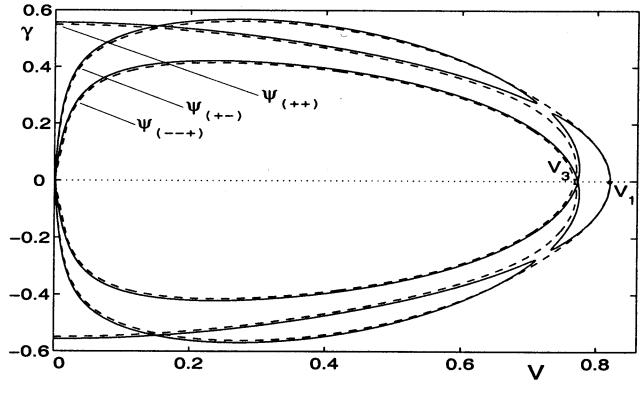

Fig. 5. The comparison of the bifurcation diagrams for $h = 0.82$ and $h = 0.8275$. Solid curve: $h = 0.8275$; dashed curve: $h = 0.82$. Although the intersection points for the dashed and solid curves do not coincide, i.e. $V_3(0.8275) \neq V_3(0.82)$ and $V_1(0.8275) \neq V_1(0.82)$, they are quite close and hence we mark them as a single point (V_3 and V_1, respectively.) The branches coming out of the point V_2 on the V-axis are omitted for visual clarity. Note the shape of the dashed and solid curves near $V \sim 0.7$, $\gamma \sim 0.3$, characteristic of phase portraits of 2D dynamical systems in the neighbourhood of saddle points.

more precisely between 0.82 and 0.8275: For $h = 0.82$ and smaller (in particular, for $h = 0.7$) the $\gamma(V)$ curve has the form of an arc shown in Fig.4(b) (i.e. it crosses the V-axis as V is increased) while for $h = 0.8275$ and greater, the curve is already loop-shaped and does not reach to $\gamma = 0$. This change of behaviour, accounting for the above 'inconsistency', is illustrated by Fig.5 which compares the $\gamma(V)$ dependencies for $h = 0.82$ and $h = 0.8275$. Fig.5 also serves to illustrate the different outcomes of the continuation of the complex $\psi_{(++)}$ for $h = 0.8353$ and smaller h. (We note that for $h = 0.8353$ the continuation of the motionless $\psi_{(++)}$ produces a pair of infinitely separated solitons ψ_+ and ψ_- (Fig.2(a)) while for $h = 0.7$, the curve departing from the same starting point $\psi_{(++)}$ ends up at the undamped asymmetric solution travelling with nonzero velocity V_3 (Fig.4(c).)

The above differences in behaviour result from the presence of a saddle point on the (γ, V)-plane, in the gap between the two lobes of the solid curve in Fig.5. Indeed, the dashed and solid curves can be seen as sections of the surface $h = h(\gamma, V)$ by the horisontal planes $h = 0.82$ and $h = 0.8275$, respectively. The gap in the upper solid curve is then accounted for by letting $h = h_0 + x^2 - y^2$ in the vicinity of the gap. Here the constant h_0 lies somewhere between 0.82 and 0.8275, and (x, y) is a pair of suitably chosen coordinates on the (γ, V)-plane.

VI. CONCLUSIONS

One of the conclusions of this work is that by grouping into complexes, solitons (or, equivalently, solitary pulses) can adjust their total momentum to zero. By doing so they can travel with nonzero speed in presence of damping — without violating the momentum decay law, $\dot{P} = -\gamma P$. Two identical solitons travelling at the same speed in the same direction have equal momenta; therefore, in order to arrange for $P = 0$ the travelling complex inevitably has to involve solitons of different varieties (i.e. both ψ_+'s and ψ_-'s.) Consequently, the real and imaginary parts of the travelling complex will always be represented by *asymmetric* functions of $\xi = x - Vt$.

Although the possibility of nondecelerated motion may be out of line with the common perception of the soliton dynamics in weakly damped Hamiltonian equations, moving pulses are not unknown in *strongly* dissipative systems. A suitable example is given by the complex Ginzburg-Landau equation. Asymmetric Ginzburg-Landau pulses, uniformly travelling with nonzero velocities, were reported in [19].

All moving solutions that we have found in this paper, turned out to be unstable. This instability admits a simple qualitative explanation — at least, for small dampings. In the undamped situation the ψ_- solitons are unstable when travelling with small velocities while the ψ_+'s become unstable when moving sufficiently fast [17]. In the presence of dissipation the travelling wave has to include solitons of both varieties; on the other hand, the eigenvalues corresponding to small nonzero γ should remain close to their ($\gamma = 0$)-counterparts. Therefore the spectrum of the travelling complex will 'inherit' unstable eigenvalues of either ψ_- (for small velocities) or of the ψ_+ (for large velocities).

Thus, despite the fact that the parametric driver can sustain the uniform motion of a damped soliton, an additional agent (such as, possibly, the diffusion and/or a nonlinear damping term) is required to make this motion stable. Here it is appropriate to refer, again, to the complex Ginzburg-Landau equation. Stable Ginzburg-Landau pulses arise as a result of a delicate balance of the whole series of terms, including dispersion, cubic and quintic nonlinearity, diffusion, cubic gain and linear and quintic nonlinear damping [19–21]. In a similar way, the gain/loss and spreading/steepening balances of the damped-driven travelling solitons could be restored by adding one or several missing agents.

Acknowledgments

We thank Nora Alexeeva for her advice on numerics. The first author's (I.B.'s) work was supported by the NRF of South Africa under grant No.2053723; by the Johnson Bequest Fund and the URC of the University of Cape Town. The second author (E.Z.) was supported by the RFBR under grant No.0301-00657; by the Visiting Lecturer's Fund of UCT, and by an NRF travel grant No.2060193.

References

[1] J.W. Miles, J. Fluid Mech. **148**, 451 (1984)

[2] C. Elphick and E. Meron, Phys. Rev. A **40**, 3226 (1989)

[3] X.N. Chen and R.J. Wei, J. Fluid Mech. **259**, 291 (1994); W. Zhang and J. Viñals, Phys. Rev. Lett. **74**, 690 (1995); W. Wang, X. Wang, J. Wang, and R. Wei, Phys. Lett. A **219**, 74 (1996); X. Wang and R. Wei, Phys. Rev. Lett. **78**, 2744 (1997); Phys. Rev. E **57**, 2405 (1998); A. Il'ichev, Physica D **119**, 327 (1998); G. Miao and R. Wei, Phys. Rev. E **59**, 4075 (1999); D. Astruc and S. Fauve. Parametrically Amplified 2-Dimensional Solitary Waves. In: IUTAM Symposium on Free Surface Flows. Proceedings of the IUTAM Symposium held in Birmingham, UK, 10-14 July 2000. A. C. King and Y. D. Shikhmurzaev, editors. Fluid Mechanics and Its Applications, Vol. **62** (Kluwer, 2001).

[4] I.H. Deutsch and I. Abram, J. Opt. Soc. Am. **B11**, 2303 (1994); A. Mecozzi, L. Kath, P. Kumar, and C.G. Goedde, Opt. Lett. **19**, 2050 (1994); S. Longhi, Opt. Lett. 20, 695 (1995); Phys. Rev. **E 55**, 1060 (1997); V.J. Sánchez-Morcillo, I. Pérez-Arjona, F. Silva, G.J. de Valcárcel, and E. Roldán, Opt. Lett. **25**, 957 (2000)

[5] I.V. Barashenkov, M.M. Bogdan, and V.I. Korobov, Europhys. Lett. **15**, 113 (1991)

[6] B. Denardo, B. Galvin, A. Greenfield, A. Larraza, S. Putterman, and W. Wright, Phys. Rev. Lett. **68**, 1731 (1992); W.-Z. Chen, Phys. Rev. **B49**, 15063 (1994); G. Huang, S.-Y. Lou, and M. Velarde, Int. J. of Bifurcation and Chaos, **6**, 1775 (1996); N.V. Alexeeva, I.V. Barashenkov, and G.P. Tsironis, Phys. Rev. Lett. **84**, 3053 (2000); W. Chen, B. Hu, H. Zhang, Phys. Rev. **B 65**, 134302 (2002)

[7] D.J. Kaup and A.C. Newell, Proc. R. Soc. Lond. A **361**, 413 (1978)

[8] I.V. Barashenkov and Yu.S. Smirnov, Phys. Rev. **E 54**, 5707 (1996)

[9] G. Terrones, D.W. McLaughlin, E.A. Overman, A. Pearlstein, SIAM J. Appl. Math. **50**, 791 (1990); I.V. Barashenkov and E.V. Zemlyanaya, Physica D **132**, 363 (1999)

[10] B.A. Malomed, Phys. Rev. A **44**, 6954 (1991); D. Cai, A.R. Bishop, N. Grønbech-Jensen, and B.A. Malomed, Phys. Rev. E **49**, 1677 (1994)

[11] I.V. Barashenkov, Yu.S. Smirnov, and N.V. Alexeeva, Phys. Rev. **E 57**, 2350 (1998); M. Kollmann, H.W. Capel, and T. Bountis, Phys. Rev. E **60**, 1195 (1999);

[12] I.V. Barashenkov and E.V. Zemlyanaya, Phys. Rev. Lett. **83**, 2568 (1999)

[13] D.J. Kaup and A.C. Newell, Phys. Rev. B **18**, 5162 (1978)

[14] C. Elphick and E. Meron, Phys. Rev. Lett. **65**, 2476 (1990)

[15] Yu.S. Kivshar and B.A. Malomed, Rev. Mod. Phys. **61**, 763 (1989)

[16] V.S. Shchesnovich and I.V. Barashenkov, Physica D **164**, 83 (2002)

[17] I.V. Barashenkov, E.V. Zemlyanaya, and M. Bär. Phys. Rev. E **64**, 016603 (2001)

[18] P. Coullet, J. Lega, B. Houchmanzadeh, and J. Lajzerowicz, Phys. Rev. Lett. **63**, 1352 (1990); P. Coullet, J. Lega, and Y. Pomeau, Europhys. Lett. **15**, 221 (1991); P. Coullet and K. Emilsson, Physica **D 61**, 119 (1992); B.A. Malomed and A.A. Nepomnyashchy, Europhys. Lett. **27**, 649 (1994); C. Elphick, A. Hagberg, B.A. Malomed, and E. Meron, Phys. Lett. **A 230**, 33 (1997); S. Longhi, Phys. Rev. **E 55**, 1060 (1997); D.V. Skryabin, A. Yulin, D. Michaelis, W.J. Firth, G.-L. Oppo, U. Peschel, and F. Lederer, Phys. Rev. **E 64**, 056618 (2001); C. Utzny, W. Zimmermann, and M. Bär, Europhys. Lett. **57**, 113 (2002); G.J. de Valcárcel, I. Pérez-Arjona, and E. Roldán, Phys. Rev. Lett. **89**, 164101 (2002)

[19] V.V. Afanasjev, N. Akhmediev and J.M. Soto-Crespo, Phys. Rev. E **53**, 1931 (1996)

[20] O. Thual and S. Fauve, J. Phys. (Paris) **49**, 1829 (1988); S. Fauve and O. Thual, Phys. Rev. Lett. **64**, 282 (1990)

[21] N. Akhmediev and A. Ankiewicz. Solitons of the Complex Ginzburg-Landau Equation. In: S. Trillo, W. Torruellas (Eds.) Spatial Solitons. Springer Series in Optical Sciences, vol. 82, 2001

Received on March 24, 2003.

Барашенков И. В., Земляная Е. В. Е17-2003-53

Движущиеся солитоны нелинейного уравнения Шредингера
с параметрической накачкой и диссипацией

Хорошо известно, что линейный диссипативный член в нелинейном уравнении Шредингера приводит к экспоненциальному затуханию импульса движущегося солитона (даже в том случае, когда осуществляется однородная по пространству подкачка энергии). Основной результат настоящей работы состоит в том, что нулевой импульс не обязательно означает нулевую скорость солитона. Показано, что в присутствии параметрической накачки два и более диссипативных солитона могут образовать комплекс, движущийся с ненулевой постоянной скоростью, но с нулевым импульсом.

На этом этапе мы обнаружили лишь неустойчивые движущиеся комплексы. Тем самым, хотя параметрическая накачка способна обеспечить равномерное движение диссипативного солитона, для стабилизации этого движения требуется присутствие дополнительных членов в уравнении.

Работа выполнена в Лаборатории информационных технологий ОИЯИ.

Препринт Объединенного института ядерных исследований. Дубна, 2003

Barashenkov I. V., Zemlyanaya E. V. E17-2003-53

Travelling Solitons
in the Damped Driven Nonlinear Schrödinger Equation

The well-known effect of the linear damping on the moving nonlinear Schrödinger soliton (even when there is energy supply via the spatially homogeneous driving) is to quench its momentum to zero. Surprisingly, the zero momentum does not necessarily mean zero velocity. We show that two or more parametrically driven damped solitons can form a complex travelling with zero momentum at a nonzero constant speed.

All travelling complexes we have found so far, turned out to be unstable. Thus, the parametric driving is capable of sustaining the uniform motion of damped solitons, but some additional agent is required to make this motion stable.

The investigation has been performed at the Laboratory of Information Technologies, JINR.

Preprint of the Joint Institute for Nuclear Research. Dubna, 2003

Макет *Т. Е. Попеко*

Подписано в печать 09.04.2003.
Формат 60 × 90/16. Бумага офсетная. Печать офсетная.
Усл. печ. л. 1,43. Уч.-изд. л. 2,15. Тираж 305 экз. Заказ № 53851.

Издательский отдел Объединенного института ядерных исследований
141980, г. Дубна, Московская обл., ул. Жолио-Кюри, 6.
E-mail: publish@pds.jinr.ru
www.jinr.ru/publish/